

Energetic Neutral Atom (ENA) intensity gradients in the heliotail during year 2003, using Cassini/INCA measurements

K. Dialynas¹, S. M. Krimigis^{1,2}, D. G. Mitchell², and E. C. Roelof²

¹Office of Space Research and Technology, Academy of Athens, 106 79 Athens, Greece.

²Applied Physics Laboratory, Johns Hopkins University, Laurel, MD, USA.

Email: kdialynas@phys.uoa.gr

Abstract. In the present study we use all-sky energy-resolved (5-55 keV) energetic neutral atom (ENA) maps obtained by the Ion and Neutral Camera (INCA) on board Cassini during the time period DOY 265/2003 to 268/2003, to investigate the properties of the peak-to-basin ENA emissions in the direction of the heliotail. Our conclusions can be summarized as follows: (1) a relatively smooth boundary (called “transition region”) between the very low (basin) and high (tail) ENA emissions from the heliosheath, with a spatial width of $\sim 30^\circ$ deg in ecl. longitude, that no theory had predicted to date, is identified in the energy range of 5-55 keV; (2) the ENA intensity gradient in this transition region is almost invariant as a function of both ecl. Latitude and energy, with an average value of $\sim 2.4\%$ per degree; (3) the deduced partial plasma pressure distributions in the 5-55 keV energy range are consistent with the ENA intensity distributions in the same energy range, while the ENA intensity gradient translates to a corresponding partial pressure gradient that occurs in the transition region; and (4) this partial pressure gradient is possibly not consistent with a tail magnetic field configuration that is similar to the measured magnetic fields by the Voyagers in the nose hemisphere.

1. Introduction

New imaging using Energetic Neutral Atom (ENA) imagers (e.g. Ion and Neutral Camera-INCA and Interstellar Boundary Explorer-IBEX) have led to new aspects of heliospheric physics and insights about heliosphere interactions with the local interstellar medium (LISM) [1],[2]. ENAs created by charge-exchange (CE) interactions in the heliosphere, can be thought of as long-distance communicators between different locations in space, i. e. their creation and detection regions. With that in mind and the knowledge of the powerful synergism between ENA measurements and in-situ energetic ion measurements by the Voyagers (e.g. [3]) a number of previously unknown parameters in the heliosphere, that were substantially at variance with theoretical models have been recently analyzed and interpreted.

The INCA detector onboard Cassini [4], capable of producing energy-resolved ENA maps of the heliosphere in the energy range of 5-55 keV, has significantly contributed to advancing our understanding on the heliosphere’s interaction with the LISM. An unexpected heliospheric signature, known as “Belt” [1], a high ENA intensity region that loops through a rough circle in the sky sphere presenting a remarkable degree of symmetry in ecliptic coordinates, has been identified in all INCA channels. The Belt was found to be energy independent in the 5-55 keV range and possibly corresponds to a reservoir of particles that exist within the heliosheath, moving in a great circle along



the nose to tail direction, passing through the ecliptic poles, constantly replenished by new particles from the solar wind, that is presumably the original source of the observed ENAs in the eV to keV energy range [5]. The high flux ENA emissions are moderately well organized in Galactic coordinates (with a $\sim 30^\circ$ tilt with respect to the galactic equator) as the ENA minima appear in the vicinity of the north and south galactic poles, but these ENA emissions are minimized in a rotated frame where its north pole points toward 190° in ecliptic longitude and 15° in ecliptic latitude.

Although a lot of effort has been expended over the past decades to estimate the overall size of the heliosphere (e.g. [6]), new analysis of the INCA ENA data [7] have shown that the heliosheath appears twice as thick along the Voyager 2 (VGR-2) line of sight (LOS; $L_{VGR2} \sim 71(+30, -15)$ AU) compared to the Voyager 1 (VGR-1) LOS ($L_{VGR1} \sim 31(+31, -18)$ AU). We know now from measurements of VGR-1 and VGR-2 that the termination shock (TS) was crossed at distances of ~ 94 AU and ~ 84 AU in 2004 and 2007, respectively [8],[9],[10],[11], while VGR-1 has probably reached the “depletion region”, i.e the interface between the solar wind plasma and the interstellar plasma, at ~ 121.6 AU [12]. These observations verify the calculations [13] (at least for the VGR-1 direction) using Cassini/INCA ENA measurements. Subsequent measurements of the plasma density in this region [14] strongly suggest that the boundary crossed is indeed the heliopause.

In the present study we re-visit the 5-55 keV INCA ENA images during the year 2003, to determine the properties of the peak to basin ENA emissions in the direction of the heliotail.

2. Instrumentation and data set information

As part of the Magnetospheric Imaging Instrument (MIMI), the Ion and Neutral Camera (INCA) onboard Cassini spacecraft is designed to perform ENA measurements originating from the vicinity of Saturn (e.g [15], [16]). INCA is a large geometry factor detector ($G \sim 0.6 \text{ cm}^2 \text{ sr}$ for H) that possesses high sensitivity to remotely detect even the lowest intensity events from large distances [4]. As shown in previous studies [1],[7], imaging of the heliosphere lies well within the instrument capabilities. The detection of the ENAs is based on the time-of-flight (TOF) technique, and several discrete energy passbands are defined within the energy range of ~ 5.2 to >220 keV. INCA utilizes a broad field of view (FOV) of 90° in the nominal Cassini roll direction (azimuthal direction) and 120° in the direction perpendicular to the spacecraft roll plane (elevational direction). The detector’s nominal angular resolution is $\sim 5^\circ$ for hydrogen (although it is energy dependent and is more than 5° for low energies).

The time period just prior to Saturn Orbit Insertion (SOI, July of 2004), provided a unique opportunity for the INCA imager to obtain neutral H images that correspond to extensive regions in the heliosphere, away from possible contaminating sources, such as Saturn’s magnetosphere. Figure 1 illustrates four all-sky (320×160 pixels), energy resolved, color-coded intensity images of heliospheric ENAs (H) in the energy range of 5–55 keV, for the time period DOY 265/2003 to 268/2003, organized in ecliptic coordinates. The data shown in this figure are the accumulation of suitable images that result from a “stare” mode of the Cassini spacecraft (i.e. the spacecraft was not rotating about its spin axis that can result in a 360° scan across the sky), where INCA FOV was pointing in the direction of the heliotail, away from the Sun, that was located towards the “nose” during that time. Blackened pixels centered at $\sim 0^\circ$ in ecliptic latitude and $\sim 30^\circ$ in ecliptic longitude correspond to the direction of Saturn and as a consequence, no observations were available for this particular region (from a distance of ~ 0.88 AU away from Saturn, the planet’s magnetosphere occupies only a few pixels in the sky, which were excluded from the analysis).

The high ENA intensities shown in figure 1 that occur in the heliotail ($\sim 60^\circ$ to 110° in ecliptic longitude and $\sim -40^\circ$ to 30° in ecliptic latitude), identified in all energy ranges, are part of the previously defined “Belt” [1] and are associated with the descending phase of solar cycle 23 (SC23) (approximately 2 yrs after the solar maximum of SC23). The general agreement between the spectra of the proton intensities inferred from the ENA measurements [17] and the Voyager ion measurements [18] suggest that the source of these ENA emissions is most likely in the heliosheath. The minima of the ENA emissions (Basin) that reside in the center of the image, at $\sim -30^\circ$ to 30° in ecliptic longitude

and -60° to 30° in ecliptic latitude, roughly coincide with the galactic South pole, with a $\sim 30^\circ$ tilt with respect to the galactic equator [6].

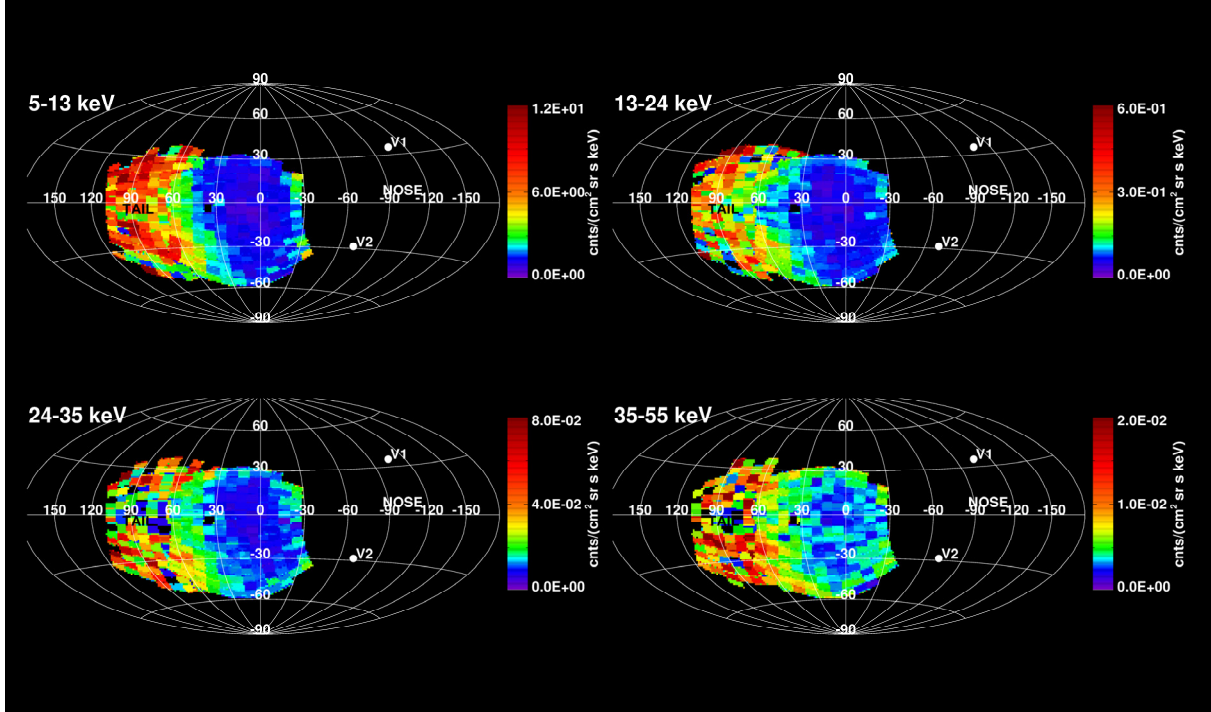


Figure 1. Intensity images of heliospheric ENAs (320x160 pixels) in the energy ranges of 5–13 keV, 13–24 keV, 24–35 keV, and 35–55 keV, organized in ecliptic coordinates (Hammer projection).

The role of all possible background sources, namely X-ray, ultraviolet, and extreme ultraviolet radiation, together with possible background from galactic Cosmic Rays (CR), have been evaluated elsewhere [1],[5] and proved to be uncorrelated with the ENA emissions that INCA detects from the heliosphere. In addition, while the Sun is located opposite of the imaging direction (i.e. no pixels are contaminated by sunlight), and the ENA emissions from Saturn’s magnetosphere are treated with exclusion criteria, we assume that our ENAs are consistent with Poisson counting statistics, i.e. all measured ENA counts C are bounded to an uncertainty of \sqrt{C} . The measured H ENA differential intensities as a function of energy ($j_{ENA} = C / (cm^2 \cdot sr \cdot s \cdot keV)$) are calculated as the LOS integral of the emission region (i.e. the heliosheath, that contains the bulk of the energetic ion population) over the intensity of the energetic ions $j_{ion}(E)$ and the interstellar flow for H-Atoms $n_H(S)$, multiplied by the energy depended charge-exchange cross section for the interaction between ion and neutral species ($\sigma^{10}(E)$).

$$j_{ENA}(E) = \sigma^{10}(E) \cdot \int_L j_{ion}(E) \cdot n_H(L) dL \quad (1)$$

As explained previously [5], the identified minima and maxima in the ENA intensities shown in figure 1, do not correspond to low and high total accumulated count regions respectively, i.e. the belt is not necessarily a high count region and becomes a high intensity region after the ENA count maps are normalized over the accumulation time per each pixel. To ensure the credibility of our results, we have averaged our original intensity maps shown in figure 1 over 11.25° in ecl. latitude and 9° in ecl.

longitude. With this averaging in intensities, the total accumulated counts found at each $11.25^\circ \times 9^\circ$ bin in the tail for the time period examined (e.g. for the 5-13 keV channel) is ~ 10 -40 counts (on average), while in the basin, the total counts per each bin is >100 counts.

3. Intensity gradients in the heliotail

One of the most interesting features in the images shown in figure 1, concerns the transition of the high ENA intensities in the tail, to the low ENA intensities in the Basin, that occurs at $\sim 60^\circ$ to 30° in ecl. longitude, henceforth called “transition region”. This region is identified in all energy ranges and serves as a relatively smooth boundary, with a spatial width of $\sim 30^\circ$ deg in ecl. longitude, between the very low and high ENA emissions in the heliosheath, that no theory had predicted to date.

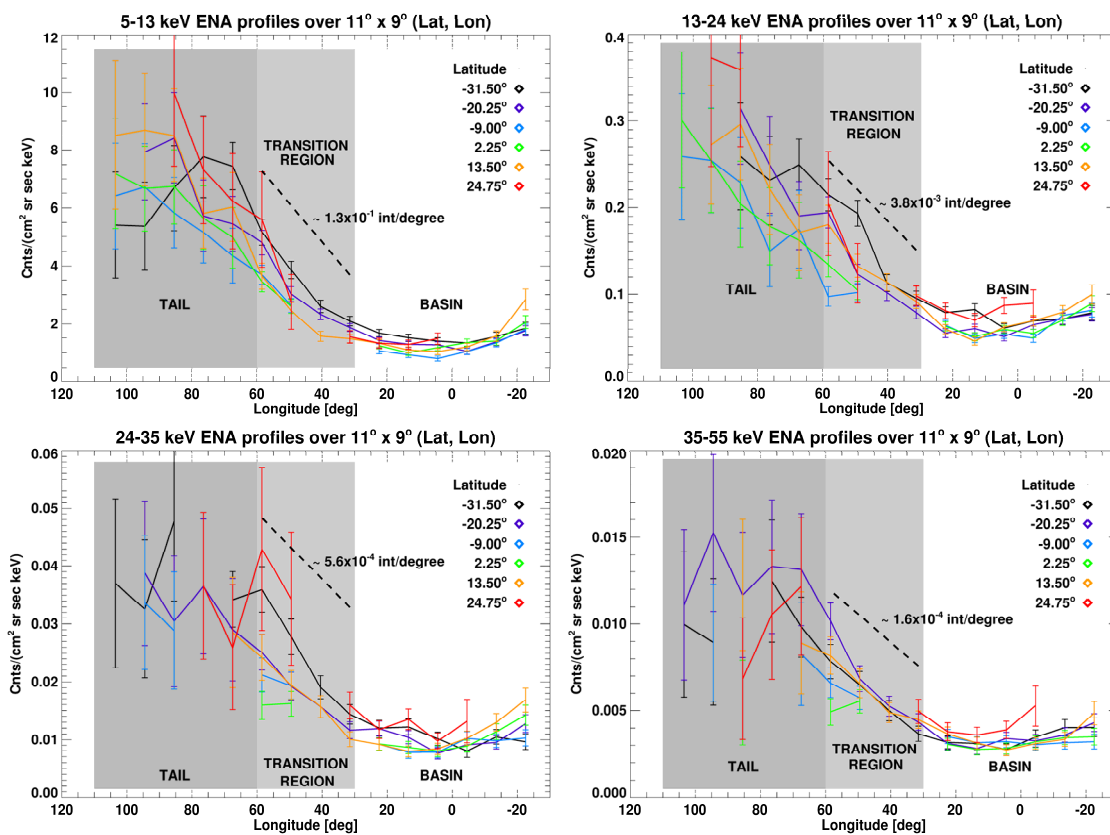


Figure 2. ENA longitudinal profiles for various latitudes in the energy range of 5-55 keV (ecliptic coordinates). Shaded grey areas are used as a visual aid to distinguish between the heliotail, the transition region and the basin. Dashed lines are average linear ENA intensity drop rates as a function of longitude, as explained in the text. Mean χ^2 values for these dashed lines are ~ 0.9 , ~ 1.8 , ~ 0.6 and ~ 0.4 for 5-13 keV, 13-24 keV, 24-35 keV and 35-55 keV channels respectively.

Although the transition region is apparent in the INCA data, it is shown fairly quiet in the low energy IBEX maps [19] and despite the fact that the 4.29 keV IBEX map [20] is very consistent with the > 5 keV INCA maps, the ENA emissions are still minimal in the transition region in that particular IBEX channel. The identified INCA “basin” is somewhat smaller in the longitude direction, while the ENA intensities in the 4.29 keV IBEX map start to build up ~ 15 - 20° closer in the tail direction compared to the > 5 keV INCA channels. Nevertheless, a similar, slightly displaced transition region between the high ENA intensities in the tail and the low ENA intensities in the so-called “offset

heliotail” (part of which is the INCA basin) is still visible in the 4.29 keV IBEX data [21]. We must keep in mind, however, that our data were taken some six years prior to the launch of IBEX, so some time variability cannot be excluded. Our primary purpose is to examine the basic properties of this unexpected, INCA defined, transition region and its possible energy dependence.

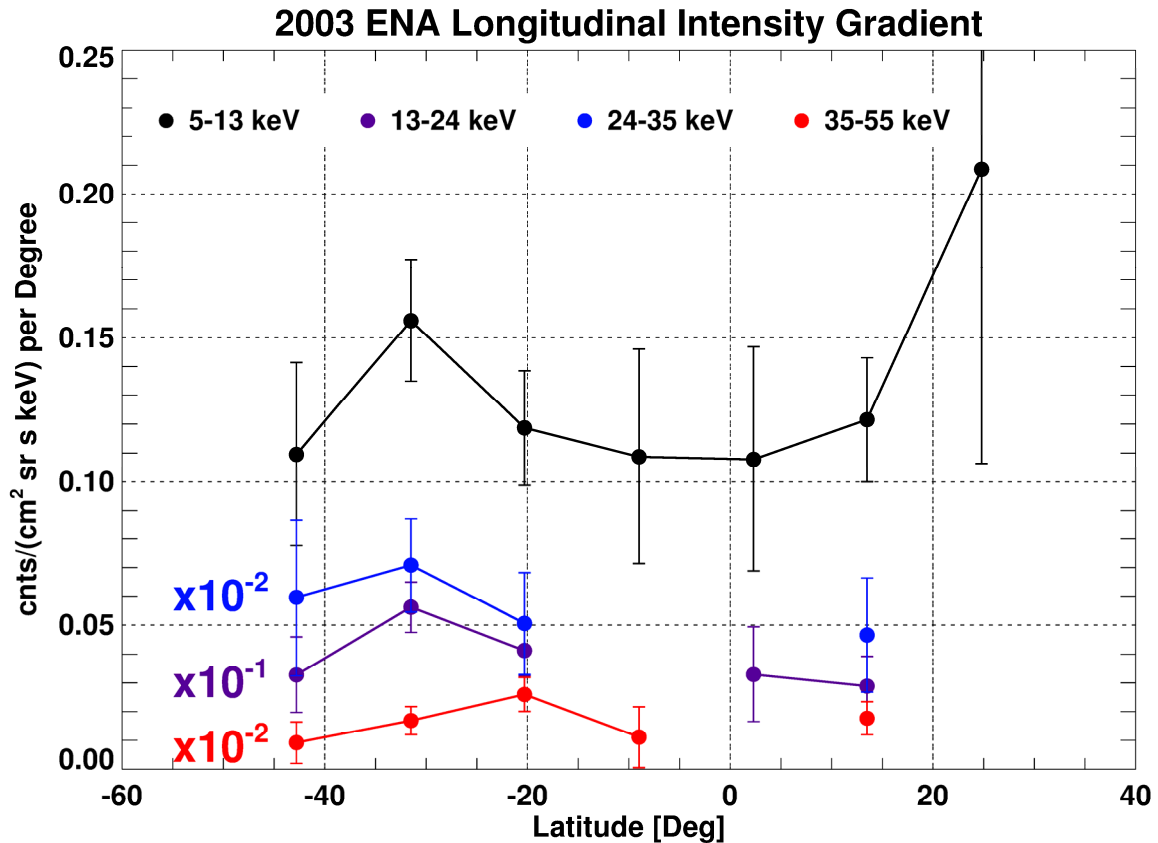


Figure 3. Longitudinal ENA intensity decrease per degree profiles as a function of Latitude that corresponds to the transition region, for all TOF channels, that resulted after fitting the $\sim 60^\circ$ to 30° in ecl. longitude ENA distributions seen in figure 2 with a linear function.

As can be seen in figure 2, the ENA intensities in the transition region drop almost linearly as a function of longitude and the basic question that needs to be answered is: How sharp is this transition region? Figure 3 shows the longitudinal ENA intensity drop rates as a function of latitude that resulted after performing normal weighted linear fits to the ENA distributions seen in figure 2, for all INCA TOF channels. Strictly speaking, these intensity drop rates represent the intensity decrease per degree that corresponds roughly to the transition region and not the “Peak to basin” intensity decrease. However, if one “extrapolates” the fitting lines (e.g. dashed lines in figure 2) to reach the longitudes where the peaks of the ENA longitudinal distributions occur, it becomes clear that these calculated rates do in fact reflect what would be the “peak to basin” intensity drop rate per each INCA TOF channel.

Given the calculated error bars, the rates shown in figure 3 are undoubtedly constant per each TOF channel as a function of ecl. latitude and an average of these rates per each channel can be adopted, corresponding to a characteristic intensity gradient rate. These characteristic intensity rates can be found in table 1 (3rd column), together with a calculation of the percentage of the intensity decrease over this 30° degree wide transition region per each TOF channel (5th column). By taking an average

of the ENA intensities at $\sim 60^\circ$ ecl. long., that corresponds to the edge of the transition region towards the tail, we conclude that the intensity gradient over this region is almost constant as a function of energy (within the calculated error bars shown in table 1) and takes an average value of $R \sim 2.4\%$ per degree.

Table 1. Transition region intensity gradient characteristic numbers.

INCA TOF channel [keV]	Average ENA intensity at $\sim 60^\circ$ ecl. Longitude [cnts/(cm ² sr s keV)]	Mean calculated rate R [cnts/(cm ² sr s keV) per degree]	Mean rate relative percentage error (dR/R %)	Percentage of Intensity decrease per degree (R%)
5-13	4.8×10^0	$(1.3 \pm 0.2) 10^{-1}$	15.4	2.8 ± 0.4
13-24	1.5×10^{-1}	$(3.8 \pm 0.5) 10^{-3}$	13.1	2.6 ± 0.3
24-35	2.7×10^{-2}	$(5.6 \pm 1.0) 10^{-4}$	17.8	2.1 ± 0.4
35-55	7.5×10^{-3}	$(1.6 \pm 0.3) 10^{-4}$	18.7	2.1 ± 0.4

The ratio of the peak ribbon flux to the underlying Globally Distributed Flux (GDF), as a function of the IBEX energy channels (e.g. in every $\sim 5^\circ$ swath of ecliptic latitude [20]) yields a number of $< 7\%$ per degree at ~ 1 keV and $< 3\%$ per degree at ~ 4 keV. As shown in the literature (e.g. [20]), the ribbon is most distinctly apparent between 1 keV and 2 keV (average width of $\sim 20^\circ$ in the 0.7 to 2.7 keV energy range), but broadens and changes its shape with increasing energy (width of $\sim 60^\circ$ at 4.29 keV) so as to match the belt as identified by INCA in the > 5 keV energy range [17],[5].

The width of the belt, as shown in the ENA emissions in the > 5 keV energy range, is almost energy independent [5]. Accordingly, the ENA intensity decrease per degree rates are almost energy independent, consistent with the ratio of the peak ribbon flux to the GDF at the 4.29 keV IBEX channel. While the < 5 keV ENA emissions, as detected by IBEX, evolve with increasing energy, the consistency between the intensity decrease rates in both the 4.29 keV IBEX channel and the > 5 keV INCA channels, provides further evidence on the concept put forward in the literature [5] concerning the interpretation of the observed global ENA heliosphere from eV to keV energy range.

4. Partial 5-55 keV INCA pressure

By taking a simpler form of equation (1), i.e. $j_{ENA} = \sigma^{10} n_H j_{ion} L_{ion}$, one can easily convert the measured ENA intensities to their parent H^+ intensities.

$$j_{H^+} = j_{ENA} / (\sigma^{10} n_H L_{ion}) \quad (2)$$

For a given H^+ momentum (p) and measured energy ΔE (INCA energy passbands), it follows [9] that we are able to calculate the partial H^+ pressure ($\Delta P = (4\pi p/3) j_{ion} \Delta E$).

$$\Delta P(pPa) = (7.0 \times 10^{-8}) \cdot v(km/s) \cdot j_{ENA} \cdot \Delta E(cm^2 \cdot sr \cdot s)^{-1} / \sigma^{10} n_H L_{ion} \quad (3)$$

Figure 4 illustrates the partial H^+ pressure for energies > 5 keV, that resulted by the use of equation (3) that is solved separately for each $11.25^\circ \times 9.0^\circ$ (ecl long. x ecl lat.) pixel of the measured ENA intensities as a function of energy, as explained in section 3. The plasma pressure distributions shown in figure 4 are very consistent with the ENA intensity distributions shown in figure 1. Namely, the high ENA intensities in the tail are associated with high partial pressures, while the partial pressures drop to minimum values in the basin. The 5-55 keV partial pressure can be calculated simply by adding the individual pressure distributions shown in figure 4. We note that the plasma pressures

shown in figure 4 are consistent with the corresponding plasma pressure calculations performed in the past [1].

Interestingly, the ENA intensity gradient shown in the transition region, translates to a partial pressure gradient in the same region for all INCA TOF channels, as shown in figure 4. Krimigis and his colleagues [1], provided a modified “diamagnetic bubble” concept concerning the shape of the heliosphere, explained earlier in the literature [22], in which the ENAs that INCA detects form a region of enhanced particle pressure inside the heliopause and contribute in balancing the pressure of the ISMF, moving the interaction with the ISMF from the TS to the HP. In situ ion measurements in the > 28 keV energy range obtained by the two Voyagers during their survey through the heliosheath, showed that the PUI pressure in the heliosheath is almost persistently higher than the magnetic field pressure [17] (i.e. plasma $\beta > 1$), which is a basic premise for the diamagnetic behavior.

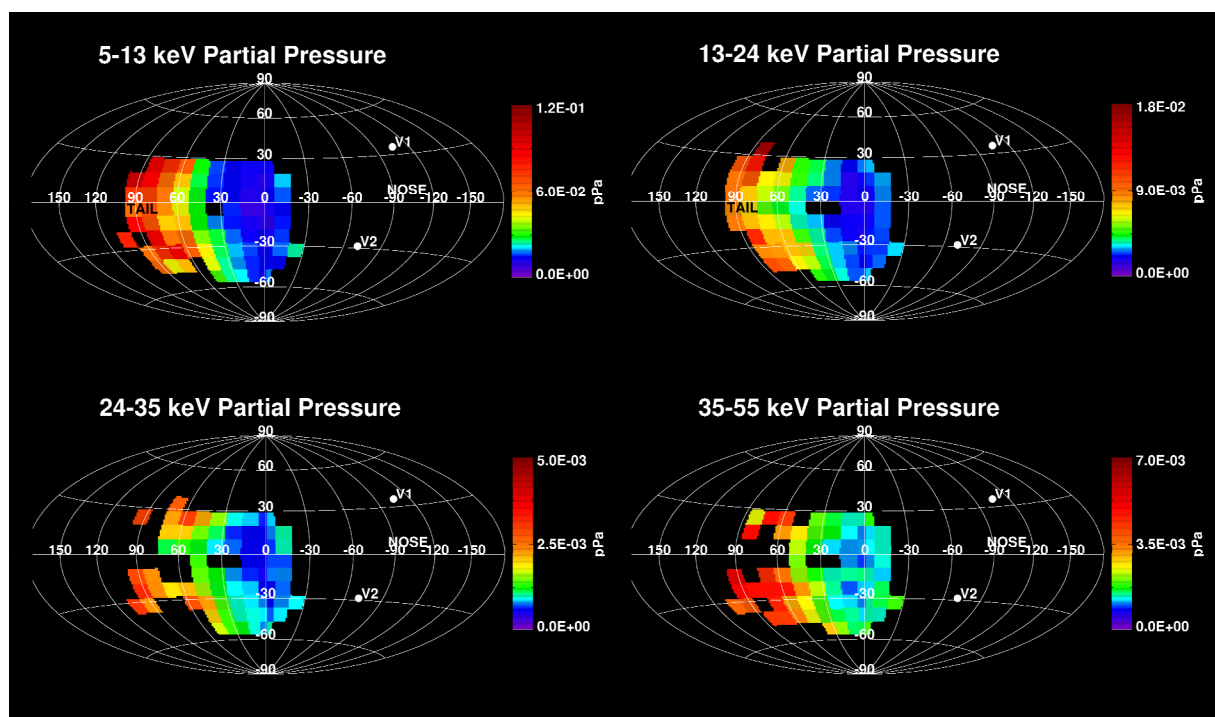


Figure 4. H^+ particle partial pressure in the 5-55 keV energy range exerted by the INCA H ENA data, assuming a heliosheath thickness of ~ 50 AU, organized in ecliptic coordinates (Hammer projection) ($1 \text{ pPa} = 10^{-11} \text{ dynes/cm}^2$). The mean relative percentage errors for these images are $\sim 14\%$ for the 5-13 keV, 13-24 keV channels and $\sim 17\%$ for the 24-35 keV, 35-55 keV channels.

In such case, the partial pressure gradient shown in figure 4 is expected to produce a “shielding current” (\vec{J}) in the heliopause that, with the assumption of isotropic pressure balance and in the absence of convection, can be expressed as follows.

$$\nabla P = \vec{J} \times \vec{B} \quad (4)$$

The 2003 INCA images indicate that the gradients of the LOS-integrated partial pressure ($5 < E < 55$ keV) in the general direction of the anti-nose (or tail) region of the heliosheath (HS) is $\partial \Delta P / \partial \varphi > 0$ (finite) and $\partial \Delta P / \partial \theta \approx 0$ (much smaller than $\partial P / \partial \varphi$). Assuming that these pressures reside in the HS, we can test against these data the implications for (or against) the existence of the simplest relation for total plasma pressure balance with the total electrical forces on the plasma, to wit, $\nabla P = \vec{J} \times \vec{B}$, which written out in the usual spherical polar coordinates becomes:

$$\left\{ \begin{array}{l} J_{\theta} B_{\varphi} - J_{\varphi} B_{\theta} = \frac{\partial P}{\partial r} \\ J_{\varphi} B_r - J_r B_{\varphi} = \frac{1}{r} \frac{\partial P}{\partial \theta} \\ J_r B_{\theta} - J_{\theta} B_r = \frac{1}{r \sin \theta} \frac{\partial P}{\partial \varphi} \end{array} \right\} \quad (5)$$

If these relations hold, they immediately imply that the total pressure gradient along the magnetic field vanishes identically, i.e. $\vec{B} \cdot \vec{\nabla} P = 0$. Therefore,

$$B_r \frac{\partial P}{\partial r} + \frac{B_{\theta}}{r} \frac{\partial P}{\partial \theta} + \frac{B_{\varphi}}{r \sin \theta} \frac{\partial P}{\partial \varphi} = 0 \quad (6)$$

Assuming that the relationships for the INCA partial pressure (ΔP) also hold (qualitatively) for the total pressure (P), then the relation among the pressure gradient components becomes:

$$\frac{\partial P}{\partial \varphi} \approx -r \sin \theta \frac{B_r}{B_{\varphi}} \frac{\partial P}{\partial r} \quad (7)$$

which cannot be influenced by B_{θ} because $\partial P / \partial \theta \approx 0$. Of course, INCA gives us no direct information on the radial pressure gradient ($\partial P / \partial r$), but nonetheless, equation (7) can be useful if we have information about the configuration of the magnetic field in the HS.

From Voyagers 1/2 (in the nose hemisphere of the HS), we know that the magnetic field is nearly Parker-like throughout the HS [23], so that $-B_r / B_{\varphi} \approx |B_r / B_{\varphi}| < 1$ (the ratio of field components is, ideally, independent of polarity). The LECP energetic ion measurements ($\sim 30 \text{ keV} < E < 1 \text{ MeV/nuc}$) indicated that the partial ion pressure at both Voyagers (ΔP) was relatively constant [24] over radial distances $\sim 30 \text{ AU}$. Thus, $r \partial \Delta P / \partial r = \Delta P (\partial \ln \Delta P / \partial r) \ll \Delta P$. On the other hand, our INCA measurements (in the anti-nose hemisphere) gave $\partial \Delta P / \partial \varphi \sim \Delta P$ over a longitude range of $\Delta \varphi \approx 30^\circ \approx 0.5 \text{ rad}$. Consequently, we can see that (given all the foregoing assumptions) if INCA is indeed measuring ENAs generated in the anti-nose hemisphere of the HS, that region cannot have a pressure distribution and a magnetic field configuration that are similar to those measured by the Voyagers in the nose hemisphere.

Equation (7) also allows us to speculate on the possibility of a non-Parker field in the anti-nose hemisphere of the HS. If the field is more tail-like, then we would have $|B_r / B_{\varphi}| > 1$, and the INCA data could be consistent with a substantial radial gradient ($\partial P / \partial r$). However, if the field had the same polarity properties as a Parker field ($-B_r / B_{\varphi} > 0$), the radial gradient would be positive (because the INCA measurement yields $\partial \Delta P / \partial \varphi > 0$), and the pressure would be increasing down the tail. In any case, equation (7), would still imply a finite radial gradient, but it would have the uncomfortable property that the sign of the radial gradient depends on the signs of the components of the (non-Parker) field in the anti-nose sector viewed by INCA.

The discussion presented here is based on several assumptions, as noted earlier, and that all contributions in our 2003 ENA image came from ENAs generated by energetic protons in the heliosheath (which, as explained earlier, is most likely). We should note that an attempt to quantitatively derive electric currents from equation (4) would be risky, because it would depend on

the assumed behavior of the magnetic field in the anti-nose hemisphere (where our ENA view is in 2003) and (even if we appeal to simulations) we have no means of independent confirmation by direct *in situ* measurements (as we have from the Voyagers in the noseward hemisphere).

5. Summary and Conclusions

By utilizing all available Cassini/INCA remote observations over the time period 265/2003 to 268/2003, we have produced all-sky, energy resolved (5–55 keV energy range) H ENA maps of the heliosphere in ecliptic coordinates. These H ENA maps were integrated over $11.25^\circ \times 9.0^\circ$ ecl. long \times ecl. lat to investigate the peak-to-basin ENA intensity gradient in the heliosheath, that translates to a corresponding tail-to-basin partial plasma pressure gradient. Primary results of this study are summarized as follows:

- A relatively smooth boundary (called “transition region”) between the very low (basin) and high (tail) ENA emissions from the heliosheath, with a spatial width of $\sim 30^\circ$ deg in ecl. longitude, that no theory had predicted to date, is identified in the energy range of 5–55 keV.
- The ENA intensity gradient in this transition region is almost invariant as a function of both ecl. latitude and energy (for >5 keV), with an average value of $\sim 2.4\%$ per degree.
- The deduced partial plasma pressure distributions in the 5–55 keV energy range are consistent with the ENA intensity distributions in the same energy range, while the ENA intensity gradient translates to a corresponding partial pressure gradient that occurs in the transition region.
- This partial pressure gradient is possibly not consistent with a tail magnetic field configuration that is similar to the measured magnetic fields by the Voyagers in the nose hemisphere.

Acknowledgments

The authors thank M. Kusterer (Johns Hopkins University Applied Physics Laboratory) for assistance with the INCA data processing. We are grateful to all colleagues on the MIMI team, who provided valuable comments that have improved the presentation. Work at JHU/APL was supported by NASA under contract NAS5 97271 and NNX07AJ69G and by subcontracts at the University of Maryland and the Office for Space Research and Applications of the Academy of Athens.

References

- [1] Krimigis, S. M., Mitchell, D. G., Roelof, E. C., Hsieh, K. C., & McComas, D. J. 2009, *Science*, 326, 971.
- [2] McComas, D. J., Allegrini, F., Bochsler, P., et al. 2009, *Science*, 326, 959.
- [3] Decker, R. B., Krimigis, S. M., Roelof, E. C. and Hill, M. E. 2012, *Nature*, 489, 124.
- [4] Krimigis, S. M., et al. 2004, *SSRv*, 114, 233.
- [5] Dialynas K., Krimigis S. M., Mitchell D. G., Roelof E. C., and Decker R. B. 2013, *ApJ*, 778:40 (13pp), doi: 10.1088/0004-637X/778/1/40.
- [6] Stone, E. C. 2001, *Science*, 293, 5527.
- [7] Roelof, E. C., Krimigis, S. M., Mitchell, D. G., Decker, R. B., & Dialynas, K. 2012, *AIP Conf. Proc.*, 1436, 239.
- [8] Decker, R. B., Krimigis, S. M., Roelof, E. C., et al. 2005, *Science*, 309, 2020.
- [9] Decker, R. B., Krimigis, S. M., Roelof, E. C., et al. 2008, *Nature*, 454, 67.
- [10] Stone, E. C., Cummings, A. C., McDonald, F. B., et al. 2005, *Science*, 309, 2017.
- [11] Stone, E. C., Cummings, A. C., McDonald, F. B., et al. 2008, *Nature*, 454, 71.
- [12] Krimigis S. M. et al. 2013, *Science*, Vol 341, pp144–147.
- [13] Krimigis, S. M., E. C. Roelof, R. B. Decker, and M. E. Hill, 2011, *Nature*, 474, pp. 359–361, doi: 10.1038/nature10115, 2011.
- [14] Gurnett, D. A. et al., 2013 *Science* 341, 1489, DOI: 10.1126/science.1241681, 2013.
- [15] Mitchell, D. G., Brandt, P. C., Roelof, E. C., et al. 2005, *GeoRL*, 32, 20501.

- [16] Dialynas, K. et al. 2013, *J. Geophys. Res. Space Physics*, 118, 3027–3041, doi:10.1002/jgra.50295.
- [17] Krimigis, S. M., Mitchell, D. G., Roelof, E. C., & Decker, R. B. 2010, in *AIP Conf. Proc.*, 1302, Pickup Ions Throughout the Heliosphere and Beyond, ed. J. Roux, G. Zank, A. J. Coates, & V. Florinski (College Park, MD: AIP), 79.
- [18] Decker, R. B., et al. 2009, in *Proc. of Twelfth International Solar Wind Conference*, Solar Wind 12, ed. M. Macksimovic, N. Meyer-Vernet, M. Moncuquet, & F. Pantellini (Sant-Malo: AIP).
- [19] Fuselier S. A. et al. 2009, *Science*, Vol 326, pp962-964.
- [20] Schwadron, N. A., Allegrini, F., Bzowski, M., et al. 2011, *ApJ*, 731, 56.
- [21] McComas, D.J. et al. 2013, *ApJ*, 771:77 (9pp), doi: 10.1088/0004-637X/771/2/77.
- [22] Parker, E. N. 1961, *ApJ*, 134, 20.
- [23] Burlaga, L. F. and N. F. Ness, 2014, *The Astrophysical Journal*, Volume 784, Issue 2, article id. 146, 14 pp. (2014).
- [24] Decker, R. B., S. M. Krimigis, E. C. Roelof and M. E. Hill, Proceedings of *This Conference*, 2014.